

Study of Dust and Ionized gas in Early-type Galaxies

Samridhi Kulkarni^a D. K. Sahu^b, Laxmikant Chaware^a,
N. K. Chakradhari^a, S. K. Pandey^a

^a*School of Studies in Physics & Astrophysics, Pt. Ravishankar Shukla University,
Raipur (C. G.), 492010, India*

^b*Indian Institute of Astrophysics, Koramangala, Bangalore 560034, India*

Abstract

We present results of optical broad-band and narrow-band H α observations of a sample of forty nearby early-type galaxies. The majority of sample galaxies are known to have dust in various forms viz. dust lanes, nuclear dust and patchy/filamentary dust. A detailed study of dust was performed for 12 galaxies with prominent dust features. The extinction curves for these galaxies run parallel to the Galactic extinction curve, implying that the properties of dust in these galaxies are similar to those of the Milky-Way. The ratio of total to selective extinction (R_V) varies between 2.1 to 3.8, with an average of 2.9 ± 0.2 , fairly close to its canonical value of 3.1 for our Galaxy. The average relative grain size $\frac{\langle a \rangle}{a_{Gal}}$ of dust particles in these galaxies turns out to be 1.01 ± 0.2 , while dust mass estimated using optical extinction lies in the range $\sim 10^2$ to 10^4 M $_{\odot}$. The H α emission was detected in 23 out of 29 galaxies imaged through narrow-band filters with the H α luminosities in the range 10^{38} - 10^{41} erg sec $^{-1}$. The mass of the ionized gas is in the range $\sim 10^3$ - 10^5 M $_{\odot}$. The morphology and extent of ionized gas is found similar to those of dust, indicating possible coexistence of dust and ionized gas in these galaxies. The absence of any apparent correlation between blue luminosity and normalized IRAS dust mass is suggestive of merger related origin of dust and gas in these galaxies.

Key words: Galaxies: early-type, individual ISM: dust, extinction, ionized gas.

Email address: samridhikulkarni2005@gmail.com (Samridhi Kulkarni).

1 Introduction

Interstellar matter (ISM), being an important factor governing the formation and subsequent evolution of galaxies, has drawn considerable attention since their detection and is still being continued to gain better understanding in various galactic and extragalactic environments. The availability of space observatories/satellites as well as ground-based telescopes with state of the art detectors has made exploration of different phases of ISM possible.

From the first detection of dust lanes in early-type galaxies (Bertola & Galletta 1978), the possibility of using its orientation to extract additional information regarding intrinsic shape of galaxies was explored (Gunn 1979; van Albada, Kotanyi & Schwarzschild 1982; Habe & Ikeuchi 1985, 1988). Importance of dust in understanding three dimensional structure of these galaxies led to search for dust in several of them (Hawarden et al. 1981; Ebneter & Balick 1985; Veron-Cetty & Veron 1988; Sadler & Gerhard 1985). Subsequently, deep optical imaging surveys of large sample of early-type galaxies detected dust in a significant fraction of them (Goudfrooij et al. 1994b; Ferrari et al. 1999). Dust has also been detected in the innermost regions of early-type galaxies in deep *Hubble Space Telescope* (HST) images, which remained unresolved with the ground-based observations (Jaffe et al. 1994; van Dokkum & Franx 1995; de Koff et al. 2000; Tran et al. 2001). Further, the detection of significant far-infrared (FIR) emission from early-type galaxies, using *Infra Red Astronomical Satellite* (IRAS), *Infrared Space Observatory* (ISO) and *Spitzer Space Telescope* has added a new dimension in the study of dust and its possible role in underlying dynamics of galaxies (Temi et al. 2004; Xilouris et al. 2004).

Optical broad-band imaging of galaxies with prominent dust features allows one to investigate physical properties of dust such as particle size, extinction, reddening, total dust content of galaxies and the processes that govern their evolution in different environments. Investigation of dust extinction in different bands *i.e.* extinction curve has been traditionally a basic tool for studying dust properties. A refined form of this technique has been applied to study the properties of dust in a number of dusty early-type galaxies (Goudfrooij et al. 1994a; Sahu et al. 1998; Patil et al. 2007; Finkelman et al. 2008, 2010). These studies showed that the extinction curves of dust in early-type galaxies run almost parallel to that of the Milky-Way, with average relative grain size not very much different from that in our Galaxy.

Optical spectroscopic observations of early-type galaxies show that $\sim 55 - 60\%$ of them have faint emission line, indicating the presence of ionized gas, with mass $\sim 10^3 - 10^4 M_{\odot}$ (Caldwell 1984, Phillips et al. 1986). Further, the H α imaging survey of large sample of early-type galaxies confirmed the presence of ionized gas with various morphologies; such as flattened disc, ring or filamen-

tary structures (Kim 1989; Shields 1991; Trinchieri & di Serego Alighieri 1991; Buson et al. 1993; Goudfrooij et al. 1994a; Singh et al. 1995; Macchetto et al. 1996; Martel et al. 2004). The possible sources of gas excitation have been explored and the post-asymptotic giant branch (pAGB) stars were identified as the main contributor of ionizing radiation. However, for at least 10% of early-type galaxies, the ionized emission is powered by recently formed stellar subcomponent (Sarzi et al. 2010).

Other forms of ISM, *i.e.* hot and cold gas have also been found in early-type galaxies. Hot gas halos have been detected around early-type galaxies with X-ray observatories (Forman, Jones & Tucker 1985; Canizares, Fabbiano & Trinchieri 1987; Fabbiano, Gioia & Trinchieri 1989; O’Sullivan, Forbes & Ponman 2001; Sarazin, Irwin & Bregman 2001; Kim & Fabbiano 2003, 2010). Cold molecular gas is detected through CO emission in $\sim 22\%$ of all early-type galaxies (Young et al. 2011 and references therein).

In a large fraction of dusty early-type galaxies, the morphology and extent of ionized gas match with that of dust (Goudfrooij et al. 1994b; Ferrari et al. 1999; Patil et al. 2007) and in some cases with the X-ray emitting region too (Goudfrooij & Trinchieri 1998). This points towards a possible physical connection between hot, warm and cold phases of ISM. The origin and fate of ISM in early-type galaxies is important as it holds clue to the formation and subsequent evolution of early-type galaxies (Goudfrooij & de Jong 1995). The recent studies have shown that neither internal nor external origin can explain all the observed properties of ISM in these galaxies. Hence, a good balance between internal and external origin is suggested as the source of ISM in early-type galaxies.

In the present paper, we discuss the properties of dust and ionized gas in a sample of forty low redshift early-type galaxies. The paper is organized as follows: Observation and data reduction in Section 2. Section 3 gives the methodology used for analyzing dust and ionized gas, the results have been discussed in Section 4. We summarize our results in Section 5.

2 Data acquisition and reduction

2.1 Observation

The aim of this work is to study the properties of dust and its relationship with ionized gas, in a large sample of early-type galaxies containing dust features. Our sample consists of 40 nearby ($z < 0.02$) early-type galaxies (E/S0) harboring some form of dust. Our program galaxies were selected from

Table 1
Global parameters of sample galaxies

Object	RA (J2000)	DEC (J2000)	Morph. (RC3)	B_T^0	V_{Helio} (km/s)	Size (arcmin)
NGC 0383	01:04:39	36:09:07	SA0	13.38	5098	1.6x1.4
NGC 0708	01:52:46	36:09:07	E	13.70	4855	3.0x2.5
NGC 0720	01:53:00	-13:44:19	E5	11.16	1745	4.7x2.4
NGC 1052	02:41:04	-08:15:21	E4	12.10	1510	3.2x2.1
NGC 1167	03:01:42	35:12:21	SA0	13.38	4945	2.8x2.3
NGC 1199	03:01:18	-15:48:29	E3	12.37	2570	2.4x1.9
NGC 1395	03:38:29	-23:01:40	E2	10.97	1717	5.9x4.5
UGC 2783	03:34:18	39:21:25	S0	12.99	6173	1.3x1.2
NGC 1407	03:40:11	-18:34:49	E0	10.70	1779	4.6x4.3
NGC 2534	08:12:54	55:40:19	E1	13.70	3447	1.4x1.2
NGC 2644	08:41:31	04:58:49	S	13.31	1939	2.1x0.8
NGC 2768	09:11:37	60:02:14	S0	10.84	1373	8.1x4.0
NGC 2851	09:20:30	-16:29:43	E	15	5195	1.2x0.5
NGC 2855	09:21:27	-11:54:34	SA	12.63	1897	2.5x2.2
NGC 3065	10:01:55	72:10:13	SA	13.5	2000	1.7x1.7
NGC 3115	10:05:14	-07:43:07	S0	09.87	663	7.2x2.0
NGC 3377	10:47:42	13:59:08	E5	11.24	665	5.2x3.0
M 105	10:47:49	12:34:54	E1	10.24	911	5.4x4.0
NGC 3489	11:00:18	13:54:04	S	11.12	677	3.5x2.0
NGC 3607	11:16:54	18:03:07	SA	10.82	960	4.9x2.5
NGC 3801	11:40:16	17:43:41	S0	12.96	3317	3.5x2.1
NGC 4125	12:08:06	65:10:27	E6	10.65	1356	5.8x3.2
NGC 4233	12:17:07	07:37:28	S0	12.8	2371	2.3x0.9
NGC 4278	12:20:06	29:16:51	E1	11.20	649	4.1x3.8
NGC 4365	12:24:28	07:19:03	E3	10.52	1243	6.9x5.0
NGC 4494	12:31:24	25:46:30	E1	10.71	1344	4.8x3.0
NGC 4552	12:35:39	12:33:23	E	10.73	340	5.1x4.7
NGC 4648	12:41:44	74:25:15	E3	12.96	1414	2.1x1.6
NGC 4649	12:43:39	11:33:09	E2	09.81	1117	7.4x6.0
NGC 4697	12:48:35	-05:48:02	E6	10.10	1241	7.2x4.7
NGC 4874	12:59:35	27:57:34	cD	12.63	7224	1.9x1.9
NGC 5322	13:49:15	60:11:26	E3	11.14	1754	5.9x3.9
NGC 5525	14:15:39	14:16:57	S0	13.6	5553	1.4x0.9
NGC 5812	15:00:55	-07:27:26	E0	12.19	1970	2.1x1.9
NGC 5846	15:06:29	01:36:20	E0	11.05	1714	4.1x3.8
NGC 5866	15:06:29	55:45:48	S0	10.74	672	4.7x1.9
NGC 6166	16:28:38	39:33:06	E2	12.78	9100	1.9x1.4
NGC 7052	21:18:33	26:26:48	E	13.40	4672	2.5x1.4
NGC 7454	23:01:07	16:22:58	E4	12.78	2022	2.2x1.6
IC 2476	09:27:52	29:59:09	S0	13.85	8007	1.5x1.4

Cols.(2) and (3) list galaxy co-ordinates, Col.(4) lists morphological classification of the galaxies, blue luminosity of the program galaxies are listed in Col.(5), while Col.(6) lists heliocentric velocity, Col.(7) optical size of the galaxies, all taken from RC3(de Vaucoulers et al. 1991)

Table 2
Details of observing runs

Run	Observatory	Instrument	Format of CCD	Scale ("/pixel)	FOV	Filters used
April 2004	IAO	HFOSC	2k × 2k	0".29	10' × 10'	<i>B, V, R, I, Hα</i>
Oct. 2004	IAO	HFOSC	2k × 2k	0".29	10' × 10'	<i>B, V, R, I, Hα</i>
Dec. 2004	IAO	HFOSC	2k × 2k	0".29	10' × 10'	<i>B, V, R, I, Hα</i>
Jan. 2005	IAO	HFOSC	2k × 2k	0".29	10' × 10'	<i>B, V, R, I, Hα</i>
March 2005	IAO	HFOSC	2k × 2k	0".29	10' × 10'	<i>B, V, R, I, Hα</i>
May 2005	IAO	HFOSC	2k × 2k	0".29	10' × 10'	<i>B, V, R, I</i>
Nov. 2005	IAO	HFOSC	2k × 2k	0".29	10' × 10'	<i>B, V, R, I</i>
Dec. 2005	IAO	HFOSC	2k × 2k	0".29	10' × 10'	<i>B, V, R, I</i>
Mar. 2008	IAO	HFOSC	2k × 2k	0".29	10' × 10'	<i>B, V, R, I</i>
	IGO	IFOSC	2k × 2k	0".3	10' × 10'	6563, 6603, 6683
April 2008	IAO	HFOSC	2k × 2k	0".29	10' × 10'	<i>B, V, R, I</i>
	IGO	IFOSC	2k × 2k	0".3	10' × 10'	6563, 6603, 6683
Aug. 2008	IAO	HFOSC	2k × 2k	0".29	10' × 10'	<i>B, V, R, I</i>
Feb. 2009	IAO	HFOSC	2k × 2k	0".29	10' × 10'	<i>B, V, R, I</i>
April 2009	IGO	IFOSC	2k × 2k	0".3	10' × 10'	6563, 6603, 6683
Oct. 2009	IGO	IFOSC	2k × 2k	0".3	10' × 10'	6563, 6603, 6683
Dec. 2009	IAO	HFOSC	2k × 2k	0".29	10' × 10'	<i>B, V, R, I</i>
Jan. 2010	IAO	HFOSC	2k × 2k	0".29	10' × 10'	<i>B, V, R, I</i>
	IGO	IFOSC	2k × 2k	0".3	10' × 10'	6563, 6603, 6683

Ebner & Balick (1985), Brown & Bregman (1998), Gonzalez-Serrano & Carballo (2000) and Tran et al. (2001). Apart from the redshift constraint and possible presence of dust in them, no strict criterion was applied for selecting the sample. The program galaxies were chosen depending on the availability of the observing time. The basic details of the sample galaxies taken from the RC3 catalog de Vaucouleurs et al. (1992) are listed in Table 1.

The observations were carried out during 2004 to 2010, using 2-m Himalayan Chandra Telescope (HCT) of Indian Astronomical Observatory (IAO), Hanle and 2-m telescope at IUCAA Girawali Observatory (IGO), Pune. Observations were made using HFOSC and IFOSC mounted on HCT and IGO, respectively. The details of the instrument used for observations in various runs are listed in Table 2. The gain and readout noise of the CCDs used are $1.22 e^-/ADU$ and $4.87 e^-$ at HCT and $1.4 e^-/ADU$ and $10 e^-$ at IGO. The seeing during our observations was between 1.0 and 2.5 arcsec. Broad-band imaging in Bessell's *B, V, R* and *I* filters for all the program galaxies were carried out with the HCT. The effective exposure time was chosen in such a way to get images with good and approximately similar signal-to-noise ratio in each band. Exposure time was split into several short exposures to avoid saturation of foreground stars and proper removal of the cosmic-ray hits. Several bias frames and twilight sky frames were also taken for pre-processing of the data.

Twenty nine out of 40 sample galaxies were also observed in narrowband $H\alpha$ filters. The $H\alpha$ filter available with the HFOSC is centered at 6563 \AA with a band-pass of 100 \AA , so relatively nearby galaxies were observed in $H\alpha$ with the HCT. The *R* band image was used for removing the overlapping continuum as suggested by Waller (1990). The IFOSC is equipped with redshifted

Table 3
Characteristics of H α filter

Filter Name	$\lambda_{cent.}$	Band-pass \AA	Peak tran. %
HCT-6563	6563	100	86%
IGO-6563	6563	80	90%
IGO-6603	6603	80	89%
IGO-6683	6683	80	88%

H α filters. The H α filter was selected according to the redshift of the galaxy and images through the adjacent narrow-band filter was taken for continuum subtraction. The details of the narrow-band filters used are listed in Table 3. Spectrophotometric standards, Hiltner 600, Feige 34 and GD140 from the list of Oke & Schwarzschild (1974), were also observed for absolute flux calibration. Details of the observations are listed in Table 4.

2.2 Data Reduction

The Image Reduction and Analysis Facility (IRAF¹) was used for data reduction. The pre-processing such as bias subtraction, flat-fielding was carried out using various tasks available within IRAF in a standard manner. Multiple frames taken in each filter were geometrically aligned to an accuracy better than one tenth of a pixel using ‘*geomap*’ and ‘*geotran*’, the aligned frames were combined to generate a final image with improved S/N ratio. This also enabled easy removal of cosmic ray events. Sky value in galaxy frame was measured within a box of size close to full width at half maximum of stellar profile, at several locations away from the galaxy. An average of these values was taken as the sky level. The sky value was also estimated by fitting a powerlaw to the outer parts of the galaxy as described in Goudfrooij et al. (1994b), results of both the methods were found to agree well. Cleaned, sky subtracted images of the program galaxies were used for further analysis.

3 Analysis

3.1 Broad-band images

Most of our sample galaxies are known to harbor dust in them, however, information regarding presence of dust in some galaxies selected from the X-ray sample of Brown & Bregman (1998), and radio sample of Gonzalez-Serrano & Carballo

¹ IRAF is distributed by the National Optical Astronomy Observatories, which are operated by the Association of Universities for Research in Astronomy, Inc., under cooperative agreement with the National Science Foundation.

Table 4
Log of observation

Galaxy Name	Total Exposure time(sec)					$H\alpha$ data	
	B	V	R	I	$H\alpha$	Cont.	HCT/IGO
NGC 0383	1500	720	540	720	NA		-
NGC 0708	3000	1200	1200	1200	5400	3600	IGO
NGC 0720	2160	1080	900	900	3600	900	HCT
NGC 1052	2100	1260	360	480	4800	4800	IGO
NGC 1167	2700	3150	2220	1200	3600	900	IGO
NGC 1199	1800	900	900	720	5700	900	HCT
NGC 1395	2400	840	540	450	2700	540	HCT
UGC 2783	3000	900	960	-	1800	960	IGO
NGC 1407	2280	1200	1080	720	4500	1080	HCT
NGC 2534	1800	900	600	600	6300	3600	IGO
NGC 2644	2400	1680	1020	900	7200	4800	IGO
NGC 2768	2100	720	720	720	4200	720	HCT
NGC 2851	2700	-	900	1200	NA		-
NGC 2855	2400	2520	840	720	5400	3600	IGO
NGC 3065	3480	1920	1500	1500	NA		-
NGC 3115	1380	480	180	60	900	180	HCT
NGC 3377	1680	900	600	510	2700	600	HCT
M 105	900	480	180	-	3600	180	HCT
NGC 3489	600	1200	900	900	5400	2700	IGO
NGC 3607	1800	900	600	-	6600	600	HCT
NGC 3801	2700	1800	800	1200	7800	800	HCT
NGC 4125	2580	780	1200	2430	1800	1200	HCT
NGC 4233	4200	2700	2100	2040	NA		-
NGC 4278	2100	1000	1200	900	NA		-
NGC 4365	2400	1200	1980	2400	3000	1980	HCT
NGC 4494	2400	1080	840	540	NA		-
NGC 4552	900	1350	-	-	NA		-
NGC 4648	3300	2640	1980	900	NA		-
NGC 4649	2280	1290	1440	-	7500	1440	HCT
NGC 4697	1200	780	600	480	1800	600	HCT
NGC 4874	2400	1200	600	540	NA		-
NGC 5322	1200	600	-	-	NA		-
NGC 5525	3600	1500	1800	2700	3600	1200	IGO
NGC 5812	-	3000	1500	-	NA		IGO
NGC 5846	1800	600	1470	1200	2400	1200	IGO
NGC 5866	2400	1040	1200	720	3000	1200	HCT
NGC 6166	1800	900	540	540	1800	1620	IGO
NGC 7052	2400	1320	1260	1200	5400	3600	IGO
NGC 7454	1440	570	105	-	4500	900	IGO
IC 2476	900	600	600	-	NA		-

(2000) is not available. So, first an attempt was made to look for possible presence of dust in these galaxies. Various image processing techniques such as colour index map, quotient image, unsharp masking etc. were used, to identify dust feature, its morphology and extent of galaxy affected by it.

3.1.1 Colour Maps

The $(B - V)$ and $(B - R)$ colour index map of the sample galaxies were created using processed and point spread function (psf) matched broad-band images. Any difference in psf in the broad-band images may lead to detection of spurious features in the colour maps. Hence, the image with better seeing

was convolved with a Gaussian kernel to match with the psf of images in other band.

While generating colour maps Goudfrooij et al. (1994c) have avoided using R filter, as H_α and [NII] emission, if present in the galaxy, lies within the R filter. It is shown by Ferrari et al. (1999) that due to the wide band-pass of R filter ($\sim 1500 \text{ \AA}$) and relatively small equivalent width of the $H_\alpha + [\text{NII}]$ emission in early-type galaxies, the contamination introduced by $H_\alpha + [\text{NII}]$ emission in the $(B - R)$ colour will be less than 1% or 0.01 mag, and hence may be neglected. As our I band images suffer from fringing (due to use of thin CCDs) and we donot have I band image for all the sample galaxies, we opted for $(B - V)$ and $(B - R)$ colour images. The colour index map of sample galaxies are displayed in Figure 1. Dust is detected in 35 out of 40 sample galaxies. We report the presence of dust in two galaxies namely, NGC 4649 and NGC 4874 for the first time. Further, we confirm the presence of dust in 33 galaxies. In our sample, 12 galaxies show dust in the form of prominent ring, lane or filaments, whereas in other cases nuclear dust patch is detected.

3.1.2 Extinction Maps

From the isophotal contours and surface brightness maps, it appears that in absence of any embedded feature, stellar light distribution of early-type galaxies is smooth. The isophotal contours of these galaxies can be well sampled by fitting ellipse on them. Presence of non-elliptical features such as dust lanes, dust patches, disk in these galaxies can distort the isophotes and they are no more perfect ellipses.

The amount of extinction caused by the dust present in galaxy is determined by comparing the light distribution of the galaxy with that expected in absence of dust. For this, ellipse fitting was carried out on the processed galaxy images using ‘*ellipse*’ task available in ‘*stsdas*’ package in IRAF, in an iterative way as mentioned by Patil et al. (2007). The ellipse fitting was first carried out for R and I band images which are least affected by the dust extinction. The center coordinate of the ellipses was determined by averaging those of the best fitted ellipses in R and I band images. This was kept fixed for fitting ellipses to the images in other bands. During the next iteration of ellipse fitting, the dust occupied regions identified with the colour index maps, were masked off to avoid the effect of distortion introduced by dust. As the extent of dust features are small compared to the size of the galaxy, masking it does not affect the fit. The deviations of isophotes from perfect ellipses, if any, are reflected in the higher order harmonics a_3 , a_4 and b_3 , b_4 . These are the amplitudes of $\sin 3\theta$, $\sin 4\theta$ and $\cos 3\theta$, $\cos 4\theta$ coefficients of the isophotal deviation from perfect ellipse. In the presence of features which distort the isophotes, the intensity distribution of early-type galaxies can be modeled well by including higher

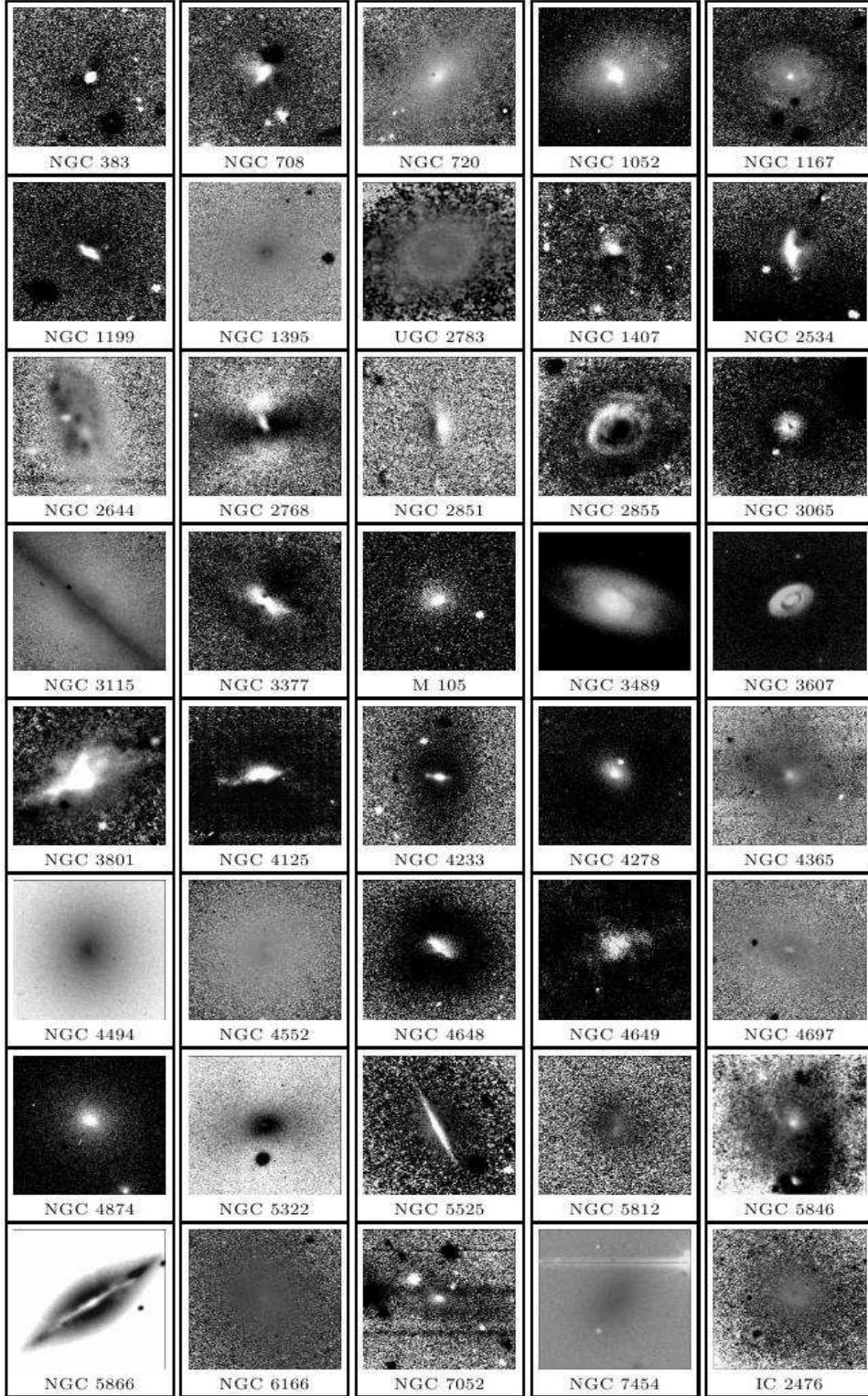


Fig. 1. $(B - R)$ Colour maps for sample Galaxies. For NGC 720, UGC 2783, NGC 3065, NGC 4278 and NGC 5812 feature was not seen clearly in $(B - R)$ we have shown $(V - R)$. Brighter shades represent dust occupied region. North is up and east is to the left.

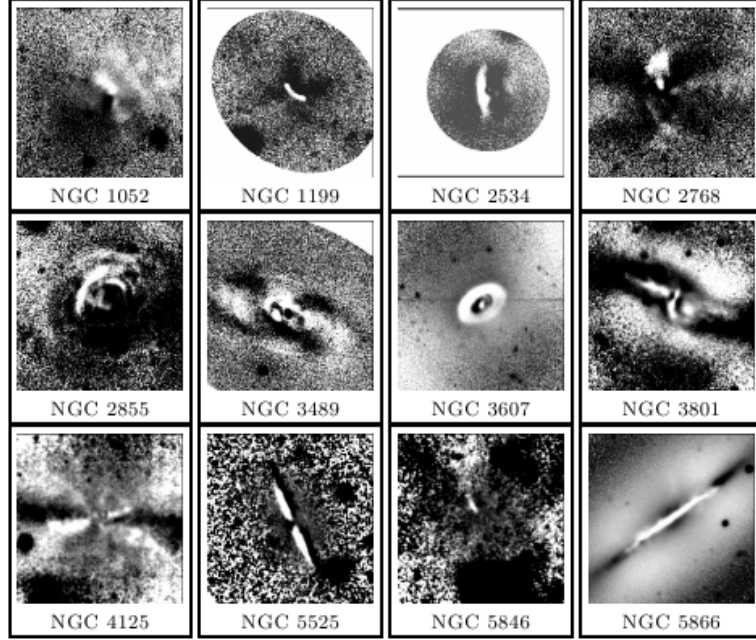


Fig. 2. Extinction map in B band for sample galaxies with prominent dust features.

order harmonics in the fit. A smooth, dust free model image of the galaxy was created by applying polynomial fit to the isophotal parameters generated by the ellipse fitting process and including the higher order harmonics using ‘*bmodel*’ task. Extinction maps in different bands were generated using the smooth dust free model of the galaxies in the following way,

$$A_{\lambda} = -2.5 \times \log \frac{I_{\lambda,obs}}{I_{\lambda,model}} \quad (1)$$

where A_{λ} represents the amount of extinction in a given band (B, V, R, I), and I_{λ} stands for the ADU counts. Figure 2 shows the extinction maps for galaxies with prominent dust feature. The almost similar morphology of dust features seen in the extinction and colour index maps supports that the identified dust features are real and not the artifact introduced by the fitting procedure. These extinction maps are then used for making extinction curves and calculating dust mass.

3.1.3 Extinction Curves

The extinction and colour index maps reveal that 12 galaxies from our sample show prominent dust features. An attempt is made to study properties of dust viz. total extinction due to dust, extinction curve, relative particle size and dust mass for these galaxies. The total extinction A_{λ} due to dust present is the only observed quantity, all other properties are directly related to it and hence proper care should be taken to determine A_{λ} . For determining A_{λ} , we

adopted the method described by Goudfrooij et al. (1994c) and Patil et al. (2007). The numerical value of total extinction A_λ ($\lambda = B, V, R$ and I), in each band was estimated by sliding a box of size comparable to that of seeing, over the dust affected part in the extinction map. The local value of selective extinction as a function of position across the dust occupied region was derived using the values of extinction A_λ measured at different locations in individual band as $E(\lambda - V) = A_\lambda - A_V$. The scatter within each box was used to estimate the uncertainty associated with the extinction values.

A linear regression fit was made between various local values of total extinction A_λ ($\lambda = B, V, R$ and I). The best fitting slope was assigned to be the average slope of A_x versus A_y and the reciprocal slope of A_y versus A_x (where $x, y = B, V, R, I$ and $x \neq y$). A similar fit was performed between the total extinction A_λ and the selective extinction $E(B - V)$, the slope gives the ratio of total to selective extinction ($R_\lambda = \frac{A_\lambda}{E(B-V)}$) for a given band (Goudfrooij et al. 1994c; Sahu et al. 1998; Patil et al. 2007). The values of R_λ thus derived for galaxies with prominent dust features are given in Table 5. The R_λ values for the Milky Way taken from Rieke & Lebofsky (1985) are also listed for comparison.

In order to study the wavelength dependence of extinction values, we plotted R_λ against λ^{-1} , known as ‘extinction curve’ and compared it with that of the Milky Way in Figure 3. The R_λ varies linearly with inverse of wavelength (λ^{-1}), consistent with the fact that extinction efficiency Q_{ext} is proportional to λ^{-1} for small grain size $x < 1$, where $x = (\frac{2\pi a}{\lambda})$ and a is grain radius. As seen in Figure 3 the extinction curves derived for dusty galaxies run parallel to that of the canonical curve of our Galaxy. This suggests that the optical extinction properties of dust grains in extragalactic environment are similar to those of the Milky Way. Finkelman et al. (2008) explored various factors which can give rise to smaller or larger values of R_λ . They concluded that increasing (decreasing) the number of upper end size grains with respect to the Galactic grain population produces larger (smaller) R_λ values. The varying abundance ratio $\frac{A_{silicate}}{A_{graphite}}$ of the silicate and graphite grains can also give rise to different values of R_λ . Since the observed abundance of silicate and graphite in the ISM is approximately equal, the variation in derived R_λ from that of the Milky Way, could only be explained due to difference in grain size. The relative dust grain size $\frac{\langle a \rangle}{a_{Gal}}$ is estimated by shifting the extinction curve as described by Hildebrand (1983), Goudfrooij et al. (1994c) and Finkelman et al. (2008). The relative dust grain size for the sample galaxies is given in Table 5.

3.1.4 Dust mass from total extinction values

To estimate dust mass in galaxies with prominent dust features, we made use of the two component model described by Goudfrooij et al. (1994c). Assuming that the dust grains are spherical with radius a , the extinction cross-section

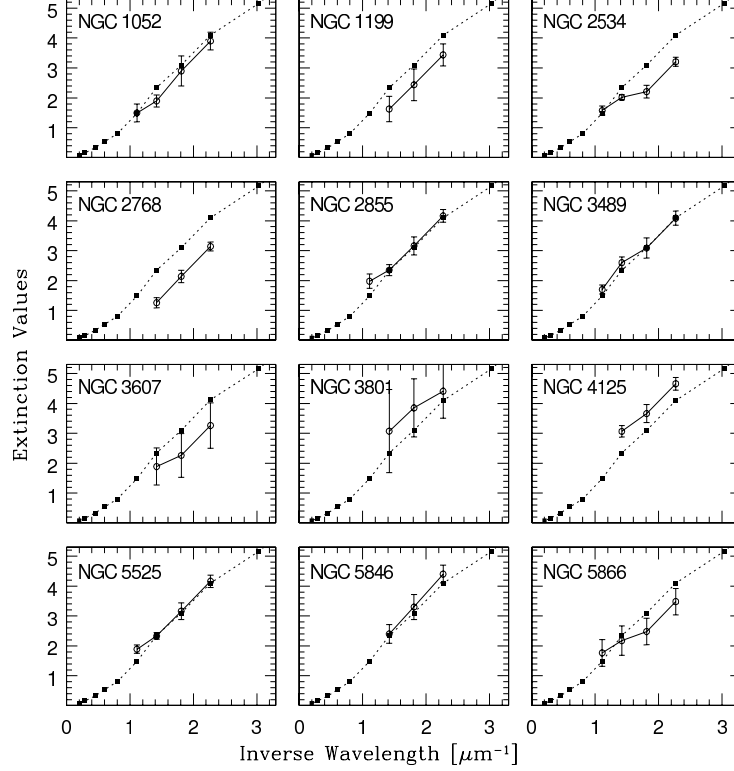


Fig. 3. Extinction curves for galaxies with prominent dust features (solid line). Extinction curve for the Milky Way (dotted line) is also plotted for comparison

Table 5

R_λ values, relative grain size and mass of dust

Object	R_B	R_V	R_R	R_I	$\frac{\langle a \rangle}{a_{Gal}}$	$\log M_{d,Opt}$
NGC						M_\odot
1052	3.9 ± 0.3	2.9 ± 0.5	1.9 ± 0.2	1.5 ± 0.3	0.94	1.8 ± 0.02
1199	3.5 ± 0.3	2.5 ± 0.4	2.2 ± 0.2	1.7 ± 0.2	0.93	2.0 ± 0.02
2534	3.1 ± 0.1	2.1 ± 0.2	2.0 ± 0.0	1.1 ± 0.1	0.83	3.3 ± 0.03
2768	3.1 ± 0.1	2.1 ± 0.2	1.3 ± 0.1	-	0.75	2.0 ± 0.01
2855	4.2 ± 0.2	3.2 ± 0.3	2.4 ± 0.1	1.9 ± 0.2	0.95	3.1 ± 0.02
3489	4.1 ± 0.2	3.1 ± 0.3	2.6 ± 0.1	1.7 ± 0.1	1.04	2.4 ± 0.05
3607	3.3 ± 0.7	2.3 ± 0.7	1.9 ± 0.6	-	0.87	2.1 ± 0.04
3801	4.4 ± 0.9	3.8 ± 0.9	3.1 ± 1.3	-	1.47	4.0 ± 0.09
4125	4.6 ± 0.2	3.6 ± 0.2	3.1 ± 0.1	-	1.36	2.1 ± 0.02
5525	4.2 ± 0.2	3.2 ± 0.2	2.3 ± 0.1	1.9 ± 0.1	1.01	4.0 ± 0.09
5846	4.4 ± 0.2	3.4 ± 0.4	2.4 ± 0.3	-	1.1	2.8 ± 0.02
5866	3.4 ± 0.4	2.5 ± 0.4	2.2 ± 0.4	1.8 ± 0.4	0.98	3.0 ± 0.09
Galaxy	4.1	3.10	2.27	1.86	1.00	

at wavelength λ is given as

$$C_{ext} = \int_{a_-}^{a_+} Q_{ext}(a, \lambda) \pi a^2 n(a) da \quad (2)$$

where $Q_{ext}(a, \lambda)$ is the extinction efficiency at wavelength λ and $n(a)$ is the grain size distribution function defined as $n(a) = n_0 a^{-3.5}$ for $a_- \leq a \leq a_+$, $a_- = 0.005 \mu m$ and $a_+ = 0.22 \mu m$ are the lower and upper cut-offs of

the grain size distribution, respectively (Mathis, Rumpl & Nordsieck 1977, Draine & Lee 1984). Under the assumption that the grain size distribution function $n(a)$ is the same over the dusty region and l_d is the dust column length along the line of sight, the total extinction A_λ is calculated as

$$A_\lambda = 1.086C_{ext} \times l_d \quad (3)$$

Integrating the dust column density Σ_d over the image area S occupied by the dust, yields dust mass in solar units as

$$M_d = S \times \Sigma_d = Sl_d \int_{a_-}^{a_+} \frac{4}{3} \pi a^3 \rho_d n(a) da \quad (4)$$

where ρ_d is the specific grain mass density $\sim 3 \text{ g cm}^{-3}$ for graphite and silicate grains (Draine & Lee 1984). The grain size obtained from the extinction curve refer to the upper end of the size distribution (Goudfrooij et al. 1994b), the upper limit of grain size a_+ for the program galaxies can be scaled as

$$a_+ = \frac{\langle a \rangle}{a_{Gal}} \times 0.22 \mu m \quad (5)$$

where $\frac{\langle a \rangle}{a_{Gal}}$ is the relative grain size, listed in Table 5 and the lower limit a_- is taken as $0.005 \mu m$. The extinction efficiencies Q_{ext} for spherical grains composed of graphite and silicate with equal abundance are taken from the published values (Jura 1982; Draine & Lee 1984). In the optical region, Q_{ext} can be parametrized as

$$Q_{ext,silicate} = \begin{cases} 0.8a/a_{silicate} & \text{for } a < a_{silicate} \\ 0.8 & \text{for } a \geq a_{silicate} \end{cases}$$

$$Q_{ext,graphite} = \begin{cases} 2.0a/a_{graphite} & \text{for } a < a_{graphite} \\ 2.0 & \text{for } a \geq a_{graphite} \end{cases}$$

with $a_{silicate} = 0.1 \mu m$ and $a_{graphite} = 0.05 \mu m$. Putting these values together, the total dust mass ($M_{d,optical}$) of the program galaxies was calculated and is listed in Table 5. While extracting the mean extinction for the sample galaxies, the dusty regions with $A_V < 0.02$ were ignored.

3.2 Dust mass using IRAS flux

Mass of dust within the galaxy can also be estimated from the IRAS flux densities by assuming thermal equilibrium. The relation between the dust

Table 6
Derived data from IRAS flux

Object	$\log L_B$ [L_\odot]	$\log L_{IR}$ [L_\odot]	$\log M_{d,IRAS}$ [M_\odot]	T_d [K]
NGC 383	10.88	9.82 ± 0.23	5.19 ± 0.24	33 ± 4
NGC 708	10.62	9.56 ± 0.26	5.07 ± 0.26	32 ± 4
NGC 720	10.52	NA		
NGC 1052	10.27	8.97 ± 0.13	4.98 ± 0.08	40 ± 1
NGC 1167	10.89	9.62 ± 0.23	6.29 ± 0.34	21 ± 2
NGC 1199	10.48	NA		
NGC 1395	10.70	8.11 ± 0.27	5.49 ± 0.58	23 ± 5
UGC 2783	10.87	NA		
NGC 1407	10.79	8.44 ± 0.22	5.02 ± 0.23	31 ± 3
NGC 2534	10.27	9.51 ± 0.23	4.95 ± 0.22	35 ± 4
NGC 2644	9.91	NA		
NGC 2768	10.70	8.89 ± 0.23	5.46 ± 0.21	31 ± 3
NGC 2851	10.33	NA		
NGC 2855	10.14	9.2 ± 0.13	5.9 ± 0.08	27 ± 1
NGC 3065	10.62	9.59 ± 0.13	4.94 ± 0.07	45 ± 1
NGC 3115	10.17	NA		
NGC 3377	9.92	7.69 ± 0.25	4.53 ± 0.29	35 ± 5
M 105	10.46	NA		
NGC 3489	9.92	NA		
NGC 3607	10.21	NA		
NGC 3801	10.42	9.68 ± 0.14	7.53 ± 0.48	16 ± 2
NGC 4125	10.74	9.08 ± 0.14	5.25 ± 0.09	36 ± 1
NGC 4233	10.12	8.83 ± 0.22	4.67 ± 0.21	35 ± 4
NGC 4278	9.99	8.42 ± 0.09	5.43 ± 0.09	32 ± 1
NGC 4365	10.59	NA		
NGC 4494	10.62	NA		
NGC 4552	10.40	7.3 ± 0.19	4.98 ± 0.26	31 ± 4
NGC 4648	9.86	NA		
NGC 4649	10.82	8.76 ± 0.1	4.73 ± 0.07	44 ± 1
NGC 4697	10.33	7.09 ± 0.93	5.17 ± 0.47	34 ± 1
NGC 4874	11.20	NA		
NGC 5322	10.78	9.05 ± 0.15	5.03 ± 0.11	36 ± 2
NGC 5525	10.58	NA		
NGC 5812	10.40	NA		
NGC 5846	10.73	NA		
NGC 5866	10.24	9.55 ± 0.14	6.58 ± 0.07	30 ± 1
NGC 6166	11.40	10.03 ± 0.21	5.81 ± 0.28	24 ± 2
NGC 7052	10.57	9.88 ± 0.15	5.37 ± 0.12	32 ± 2
NGC 7454	10.18	NA		

mass and the observed far-IR flux density I_ν , is

$$M_d = \frac{4}{3} a \rho_d D^2 \frac{I_\nu}{Q_\nu B_\nu(T_d)} \quad (6)$$

where a is grain radius, ρ_d is specific grain mass density, D is distance of the galaxy in Mpc, Q_ν and $B_\nu(T_d)$ are the grain emissivity and Planck function at temperature T_d and frequency ν , respectively (Hildebrand 1983). The temperature of dust was calculated following Young et al. (1986b); Patil et al. (2007)

$$T_d = 49(S_{60}/S_{100})^{0.4} \quad (7)$$

where S_{60} and S_{100} are the flux densities at $60\mu\text{m}$ and $100\mu\text{m}$. The calculated dust temperature is listed in Table 6. The estimated dust temperatures should

be regarded as ‘representative’ values, since a *range* of temperature is appropriate for dust within early-type galaxies (Goudfrooij & de Jong 1995). The value of T_d varies from 26 K to 39 K indicating possible presence of ‘warm’ dust in these galaxies.

It is shown by Mathis & Wallenhorst (1981) that the observed extinction curve of the Milky Way is not consistent with attenuation of starlight by uniform grain size and hence the grain size a and grain emissivity Q_ν need to be suitably chosen averages. For obtaining the average grain emissivity, the value for each grain is weighted by the contribution of the grain to the flux density and hence by grain volume. Similarly, for a given size distribution, an average value of a can also be obtained by weighted average. For particle size distribution function of Mathis, Rumpl & Nordsieck (1977), a weighted average radius a of $0.1 \mu\text{m}$ was calculated by Hildebrand (1983). Hence, in this study we have taken average grain size of $0.1 \mu\text{m}$, $\rho_d = 3 \text{ g cm}^{-3}$ and $\frac{4a\rho_d}{3Q_\nu} = 0.04 \text{ g cm}^{-2}$ at $100 \mu\text{m}$ (Hildebrand 1983). The dust mass for galaxies with available IRAS fluxes obtained following the method outlined in Thronson & Telesco (1986) and Goudfrooij et al. (1994b) is listed in Table 6.

3.3 Narrow-band images

A significant fraction ($\sim 75\%$) of our sample was observed with narrowband $\text{H}\alpha$ filter for studying properties of ionized gas. The images obtained through $\text{H}\alpha$ filter include photons from $\text{H}\alpha + [\text{NII}]$ lines and from the underlying continuum. Pure $\text{H}\alpha$ line emission map of sample galaxies can be generated as described below.

The $\text{H}\alpha$ and continuum images were first geometrically aligned and combined to get the final narrow-band and continuum images. The image with better seeing was convolved to match the psf of narrow-band and continuum images. A scaled version of the continuum image is subtracted from the narrow-band image to get pure $\text{H}\alpha + [\text{NII}]$ emission-line image. The intensity scaling factor (ISF) was obtained following the method described by Spector, Finkelman & Brosch (2012). Under the assumption that mix of foreground stars represents the stellar population of program galaxy, mean of ratio of fluxes of the foreground stars in line and continuum images was used as the scaling factor. The continuum subtracted images shows presence of line emission in many of our sample galaxies. Spector, Finkelman & Brosch (2012) also cautioned that regardless of number of stars taken for estimating ISF, it is very difficult to match the stellar population of the observed galaxy with that of the foreground stars.

An alternate method to estimate the ISF was also tried. In this method ellipses

were fitted to the isophotes of galaxies in both the bands. A least square fit was applied to the intensities measured in outer regions of narrow-band and continuum images, which was minimally affected by the ionized gas. The slope of this fit gives the scale factor between continuum and emission line images (Macchetto et al. 1996). Intercept of the least square fit is related to the residual in the sky background between the two bands, an accurate sky subtraction reduces the intercept of the fit to zero. The accuracy of ISF was checked by examining the continuum subtracted images which are expected to show zero value in the outer regions and clean removal of the foreground stars. The ISF so obtained were compared with those estimated using the foreground stars. For a good number of galaxies, the two ISFs agreed well, in case of discrepant values, the second method being more accurate was preferred.

The resultant images were examined visually for possible presence of line emission. Line emission is detected in 23 out of 30 galaxies imaged through narrow-band filter. In most of the line emitting galaxies the emission is centered around the nucleus. The total $H\alpha + [NII]$ counts $N_{H\alpha+[NII]}$ inside a circular aperture centered on the galaxy nucleus was estimated using ‘DAOPHOT’ in IRAF. The aperture size was taken big enough to encompass all the line emission from the galaxy. The final aperture sizes used for the count measurement are given in Table 7.

The line emission maps of our sample galaxies with detectable line emission are displayed in Figure 4. The measured $H\alpha + [NII]$ counts were converted to absolute flux scale using the following relation

$$F_{\alpha}(\text{erg cm}^{-2} \text{ s}^{-1}) = C_{\alpha} \times f_{\alpha}(\text{count s}^{-1}) \quad (8)$$

where C_{α} the conversion factor was determined by comparing the observed counts (f_{α}) of the spectrophotometric standard star with the expected flux (F_{α}) within the bandpass of the filter used. Pure $H\alpha$ flux can be estimated from the observed flux by removing the contamination due to $[NII]$ lines using the correction factor

$$Corr. = \frac{1}{1 + [NII]Cont. \times \frac{[NII]}{H\alpha} \times 1.33} \quad (9)$$

where $[NII]$ Cont. is contamination due to the $[NII]$ lines and estimated as the ratio of the average transmission efficiency of the filter at $\lambda\lambda 6548, 6583$ to that of $H\alpha$. The $\frac{[NII]}{H\alpha}$ ratio for a galaxy is usually determined spectroscopically. In absence of spectroscopic information the value of $\frac{[NII]}{H\alpha}$ was taken as 1.38 (Phillips et al. 1986). The derived $[NII]$ contamination, correction factor and pure $H\alpha$ flux are given in Table 7. The $H\alpha$ luminosities for the sample galaxies were calculated using the distance derived from the velocities corrected for local group infall onto Virgo (source Hyperleda) and Hubble constant $H_0 =$

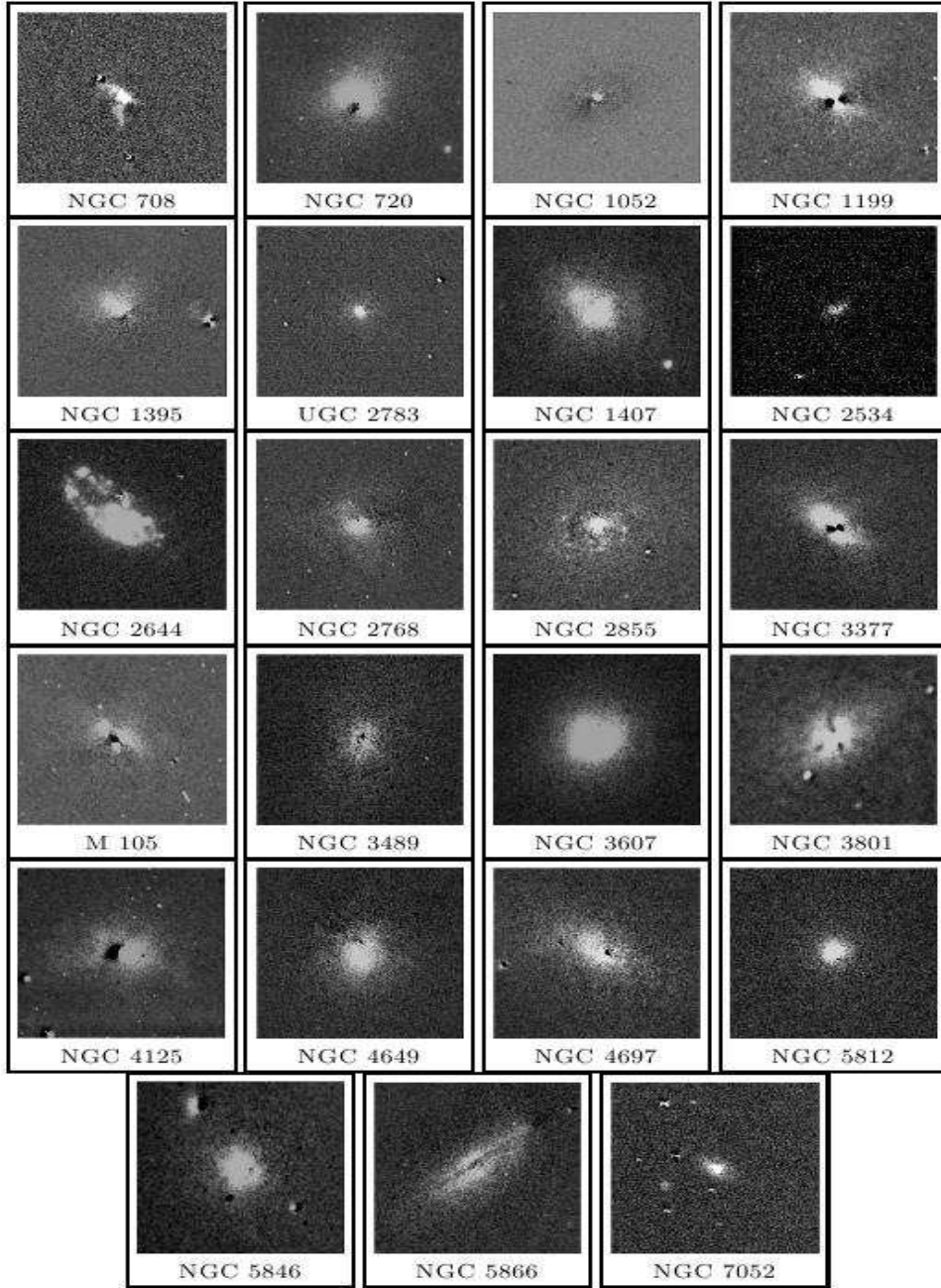


Fig. 4. $H\alpha$ Emission Map for sample Galaxies.

$73 \text{ km sec}^{-1} \text{ Mpc}^{-1}$ (Spergel et al. 2007).

3.3.1 Mass of ionized gas

The mass of ionized gas M_{HII} was estimated following Goudfrooij et al. (1994b) and Macchetto et al. (1996), using the relation,

Table 7
Results for $H\alpha + [NII]$ emission

Object name	Dist. Mpc	Aper. arcsec	[NII] contam-ination	Corr.	$f_{H\alpha}$ 10^{-14} $erg\,cm^2\,s^{-1}$	$L_{H\alpha}$ $erg\,s^{-1}$	$\log M_{HII}$ M_{\odot}	Remarks on dust and IG morphology
NGC0708	68.92	4	0.99	0.355	0.39	2.22×10^{41}	5.71	Marginal dust in central region
NGC0720	22.16	29	0.79	0.408	15.7	9.22×10^{39}	4.33	Nuclear dust & IG in center
NGC1052	19.10	26	0.82	0.399	22.4	9.77×10^{39}	4.35	Nuclear dust & IG in center
NGC1167	70.23		No Emission					Dust patch
NGC1199	35.20	32	1.32	0.291	3.5	5.19×10^{39}	4.08	Marginal dust in central region
NGC1395	21.07	20	0.80	0.405	3.91	2.08×10^{39}	3.68	Small dust lane along minor axis
UGC2783	87.39	19	0.77	0.414	2.72	2.48×10^{40}	4.76	IG in center region
NGC1407	22.57	43	0.78	0.411	18.0	1.10×10^{40}	4.40	IG in center
NGC2534	51.74	6	0.62	0.468	1.13	3.62×10^{39}	3.92	Marginal IG in central region
NGC2592	29.44		No Emission					DL along major axis
NGC2644	26.63	41	0.94	0.367	13.3	1.13×10^{40}	4.42	Dust patch & IG near center
NGC2768	22.52	26	0.76	0.418	6.9	4.19×10^{39}	3.98	Dust patch & IG near center
NGC2855	24.96	42	0.94	0.367	9.7	7.23×10^{39}	4.22	Spiral like filaments dust & IG filaments
NGC3115	8.15		No Emission					no dust
NGC3377	10.34	35	0.90	0.377	7.24	9.26×10^{38}	3.33	Dust & IG along major axis
M105	13.36	26	0.90	0.377	8.03	1.71×10^{39}	3.60	IG in center
NGC3489	10.68	25	0.73	0.427	15.2	2.07×10^{39}	3.68	Warped dust & IG feature
NGC3607	14.17	35	0.90	0.377	35.0	8.40×10^{39}	4.29	Dust & IG ring around center
NGC3801	49.27	35	1.1	0.331	4.64	1.35×10^{40}	4.49	Multiple DL & filamentary structure of IG
NGC4125	22.98	49	0.76	0.418	14.1	8.91×10^{39}	4.31	Small dust lane & IG in central region
NGC4365	17.84	35	No Emission					Dust patch
NGC4649	16.64	32	0.80	0.405	9.79	3.24×10^{39}	3.87	Nuclear dust; IG in center
NGC4697	2.80	49	0.81	0.402	31.8	2.98×10^{38}	2.84	Dust patch & IG in center
NGC5525	78.62		No Emission					Large dust lane along Major axis
NGC5812	27.13	23	0.92	0.372	25.3	2.23×10^{40}	4.71	Dust patch & IG in center
NGC5846	25.45	23	0.97	0.360	18.9	1.46×10^{40}	4.53	Nuclear dust patch & IG in center
NGC5866	13.20	41	0.88	0.382	10.7	2.23×10^{39}	3.71	Large dust lane & associated IG
NGC6166	132.53		No Emission					No dust
NGC7052	67.53	17	0.99	0.355	0.74	4.04×10^{39}	3.97	Small dust patch & IG in center
NGC7454	29.04		No Emission					No dust

$$M_{HII} = 2.33 \times 10^3 \left(\frac{L_{H\alpha}}{10^{39}} \right) \left(\frac{10^3}{n_e} \right) M_{\odot} \quad (10)$$

where $L_{H\alpha}$ is the $H\alpha$ luminosity. The derived mass of ionized gas is listed in Table 7. The uncertainty in the emission line flux measurement is discussed in detail by Macchetto et al. (1996). The main source of error is the uncertainty involved in determination of ISF which depends on the equivalent width of the ionized-gas emission. Hence, the measurement error is more for the galaxies with faint and diffuse emission. However, other sources like photon-noise in the narrow-band and continuum images, residual spatial variation after flat-fielding, error in sky subtraction, inaccurate psf matching of the narrow-band and continuum images etc. also contribute to the final error. Typical error in our $H\alpha + [NII]$ flux measurement is $\sim 20\%$.

4 Results and Discussion

Dust: For the galaxies with obvious features of dust extinction, it is found that morphology and extent of the dust feature in colour-index image is similar to that of extinction map. This indicates that the extinction map approximates the dust obscured region to a high degree. An analysis of extinction curves for 12 galaxies is presented in this work. The extinction curves for eight galaxies are reported for the first time. The value of R_V and relative grain size for the sample galaxies obtained by analyzing the extinction maps are given in Table 5. The value of R_V for sample galaxies varies from 2.1 to 3.8 with an average of 2.95. It is close to the previously reported values by Goudfrooij et al. (1994c) ($R_V = 2.7$), Patil et al. (2007) ($R_V = 3.01$) and Finkelman et al. (2010) ($R_V = 2.82$). We find that the galaxies having R_V values less than the canonical value of 3.1 have well settled dust morphology in the form of a dust lane or a ring and have relatively smaller grain size than that of the Milky Way. Conversely, the galaxies with larger values of R_V show irregular dust morphology and larger relative grain size. This result is in good agreement with results of Goudfrooij et al. (1994b), Patil et al. (2007) and Finkelman et al. (2010). There are four galaxies in common with the samples of Goudfrooij et al. (1994c) and Patil et al. (2007). Table 8 presents the value of R_V , relative grain size and optical dust mass for the four common galaxies along with the previously reported values in the literature. Except for galaxy NGC 4125, which shows complex dust structure (Goudfrooij et al. 1994c), our results are in good agreement with those reported in the literature.

Goudfrooij et al. (1994b) explored various dust destruction mechanisms such as sputtering of dust by supernova blast wave, turbulent shocks, thermal ions and hot gas etc. It is shown that for volatile grain of radius $\sim 0.1 \mu\text{m}$, the lifetime of dust grain varies from 10^7 to 10^9 years. The mass of dust and its grain size are expected to drop gradually with time since the dust was acquired by the galaxy. In this scenario, the smooth and regular dust lane morphology associated with smaller grain size is expected, if the galaxy had sufficient time for the dust to settle down in a regular shape. On the other hand if the dust is acquired recently, it will lack regular dust morphology as in the case of NGC 3801. Among our sample galaxies NGC 3801 shows considerably larger relative grain size (1.47) and larger value of R_V . A multiwavelength study of this galaxy by Hota et al. (2012) revealed that this galaxy has a kinematically decoupled core or an extremely warped gas disc, dust filaments with complex structures, recent star burst with age less than 500 Myr and evidence of ionized gas (as seen in this study too). All these facts led Hota et al. (2012) to suggest that this galaxy is a merger-remnant early-type galaxy. The results of Hota et al. (2012) support that NGC 3801 acquired dust in the recent past and did not have enough time to settle it into a smooth, regular morphology, which may result in the observed larger grain size and R_V value, as suggested

Table 8

Comparison of dust properties

Galaxy Name	This Paper			Reported values for comparison			
	R_V	$\frac{\langle a \rangle}{a_{Gal}}$	$\log(\frac{M_{d,opt}}{M_\odot})$	R_V	$\frac{\langle a \rangle}{a_{Gal}}$	$\log(\frac{M_{d,opt}}{M_\odot})$	Reference
NGC 2534	2.1 ± 0.20	0.83	3.32 ± 0.03	2.03 ± 0.28	0.80	3.78	Patil et al. (2007)
NGC 3489	3.1 ± 0.33	1.04	2.40 ± 0.05	3.38 ± 0.21	1.09	3.66	Patil et al. (2007)
NGC 4125	3.6 ± 0.27	1.36	2.10 ± 0.02	2.74 ± 0.33	0.96	5.22	Goudfrooij et al. (1994c)
NGC 5525	3.2 ± 0.28	1.01	4.04 ± 0.09	3.15 ± 0.17	0.99	5.67	Patil et al. (2007)

by Goudfrooij et al. (1994c).

The dust mass reported in this work using optical extinction is in the range $10^2 - 10^4 M_\odot$ while, the dust mass estimated using IRAS fluxes is higher by a factor of $\sim 10^2$. This indicates that a significant fraction of dust is diffusely distributed throughout the galaxy (Goudfrooij & de Jong 1995; Wise & Silva 1996) which could not be detected with optical observations, this is in agreement with that of previous studies (Patil et al. 2007; Finkelman et al. 2008, 2010).

Ionized gas: $H\alpha$ line emission is detected in $\sim 85\%$ of our sample galaxies observed in narrow-band, the results are listed in Table 7. The $H\alpha$ luminosity of the sample galaxies lies in the range $10^{38} - 10^{41} \text{ erg sec}^{-1}$ and the mass of ionized gas lies in the range $\sim 10^3 - 10^5 M_\odot$. The ionized gas and dust have identical morphology in almost all the galaxies detected in $H\alpha$ (refer Figure 2 and 4). We have several galaxies in common with earlier studies by Kim (1989), Trinchieri & di Serego Alighieri (1991), Shields (1991), Goudfrooij et al. (1994b), Macchetto et al. (1996) and Finkelman et al. (2010). The $H\alpha$ flux estimated in this work are in good agreement with the flux reported in the literature (refer Table 9). There are 6 galaxies for which $H\alpha$ flux are available from more than one source and a significant scatter is noticed among them. The source of scatter may be due to the higher uncertainty involved in the method of determination of the line emission fluxes as discussed in Section 3.3. Similar discrepancy in $H\alpha$ flux was also reported by Finkelman et al. (2010).

4.1 Association of dust and ionized gas

Association of dust and ionized gas and their possible origin in E/SO galaxies were studied recently by Finkelman et al. (2012). The HST observations revealed presence of nuclear and filamentary/patchy dust in the central part of a significant fraction of early-type galaxies (Tran et al. 2001; Martel et al. 2004). Most of the galaxies from our sample show dust in their central part. A study similar to that of Finkelman et al. (2012) was carried out, by including early-type galaxies with nuclear, filamentary/patchy dust to the sample of galaxies having dust lanes. Various relevant parameters like optical dust mass,

Table 9
Comparison of $H\alpha$ fluxes

Galaxy name	$f_{H\alpha}$ This paper $ergcm^2s^{-1}$	Other obs. $ergcm^2s^{-1}$	Reference
NGC0708	39×10^{-14}	49×10^{-14}	Finkelman et al. (2010)
NGC0720	15.7×10^{-14}	$< 1.49 \times 10^{-14}$ $< 3.53 \times 10^{-14}$ 17.66×10^{-14}	Goudfrooij et al. (1994b) Shields (1991) Macchetto et al. (1996)
NGC1052	22.4×10^{-14}	8.1×10^{-14}	Kim (1989)
NGC1199	3.5×10^{-14}	4.9×10^{-14}	Finkelman et al. (2010)
NGC1395	3.91×10^{-14}	2.2×10^{-14} 22.7×10^{-14} 9.33×10^{-14}	Goudfrooij et al. (1994b) Macchetto et al. (1996) Trinchieri & di Serego Alighieri (1991)
NGC1407	18.0×10^{-14}	0.9×10^{-14} $< 5.11 \times 10^{-14}$ 4.82×10^{-14}	Goudfrooij et al. (1994b) Shields (1991) Macchetto et al. (1996)
NGC2534	1.13×10^{-14}	6.4×10^{-14}	Finkelman et al. (2010)
NGC3377	7.24×10^{-14}	11.9×10^{-14}	Goudfrooij et al. (1994b)
NGC3489	15.2×10^{-14}	51.89×10^{-14}	Macchetto et al. (1996)
NGC3607	35.0×10^{-14}	7.83×10^{-14}	Macchetto et al. (1996)
NGC4125	14.1×10^{-14}	39.5×10^{-14} 16×10^{-14}	Goudfrooij et al. (1994b) Kim (1989)
NGC4649	9.79×10^{-14}	11×10^{-14}	Trinchieri & di Serego Alighieri (1991)
NGC4697	31.8×10^{-14}	29.5×10^{-14} 4.7×10^{-14}	Goudfrooij et al. (1994b) Trinchieri & di Serego Alighieri (1991)
NGC5812	25.3×10^{-14}	5.83×10^{-14}	Macchetto et al. (1996)
NGC5846	18.9×10^{-14}	16×10^{-14} 28.02×10^{-14}	Trinchieri & di Serego Alighieri (1991) Macchetto et al. (1996)
NGC7052	0.74×10^{-14}	6.0×10^{-14}	Finkelman et al. (2010)

IRAS dust mass, ionized gas mass, optical luminosity, IR luminosity, $H\alpha$ luminosity etc. were collected from Buson et al. (1993), Goudfrooij et al. (1994b), Goudfrooij & de Jong (1995), Sahu et al. (1996) Sahu et al. (1998), Dewangan, Singh & Bhat (1999), Singh et al. (1995), Tran et al. (2001), Patil et al. (2007), Finkelman et al. (2010), Finkelman et al. (2012), this we denote as combined sample. Wherever necessary the quantities have been normalized for $H_0 = 73 \text{ km sec}^{-1} \text{ Mpc}^{-1}$.

The lower optical depth and smaller sampling area in galaxies with patchy/filamentary dust makes it difficult to determine dust mass using extinction values. Dust mass using optical extinction could be estimated only for 12 galaxies with prominent dust features in our sample. It was demonstrated by Tran et al. (2001) that even in the case of patchy/filamentary dust, the dust mass determined using optical extinction and IRAS fluxes are well correlated. Further, the ionized gas mass and optical dust mass are found to be correlated in early-type galaxies (Ferrari et al. 1999; Finkelman et al. 2012). The slope of $\log(M_{HII})$ versus $\log(M_{dust,opt})$ for the combined sample was found to be ~ 0.6 , which is shallower than the slope (~ 0.8) found by Finkelman et al. (2012) for dust lane galaxies. This indicates that in the prominent dust lane galaxies the source of ionization may be more efficient compared to the galaxies with patchy/filamentary dust.

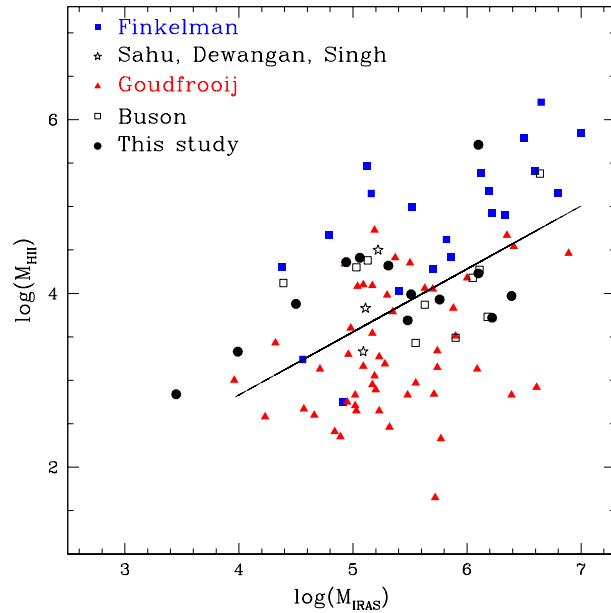


Fig. 5. Ionized gas mass plotted versus dust mass estimated from *IRAS* fluxes

In Figure 5 dust mass derived using *IRAS* fluxes is plotted versus ionized gas mass. A good correlation between these two quantities is seen. The best fitting line to the observed data points with slope ~ 0.72 is also shown in the same figure. Our results about the co-existence of dust and ionized gas and their correlation are consistent with those of similar work by Goudfrooij et al. (1994b), Goudfrooij & de Jong (1995), Macchetto et al. (1996) and Finkelman et al. (2008, 2010).

4.2 Possible source of ionization in early-type galaxies

The common presence of ionized gas in early-type galaxies is well established (Kim 1989; Goudfrooij et al. 1994b; Macchetto et al. 1996; Sarzi et al. 2006; Finkelman et al. 2008), however, the source of ionization is still debated. Possible sources of ionization in early-type galaxies were investigated (Martel et al. 2004; Sarzi et al. 2010). Sarzi et al. (2010) explored various possible sources of ionization e.g. post-asymptotic giant branch (pAGB) stars, presence of AGN's, fast shocks, OB stars and interaction with hot ISM. On the basis of their ionizing balance arguments the pAGB stars were regarded as the best candidate for photoionization; it may be either associated to old stellar population or to recent star formation. However, on-going star formation is also responsible for ionization of gas in at least $\sim 10\%$ of their sample.

The GALEX ultraviolet data revealed that the strong UV flux from $\sim 30\%$ of nearby bright early-type galaxies can not be explained without invoking \sim

1 - 3% (in total stellar mass) star formation rate in the last billion years. The fraction of galaxies showing recent star formation could be as high as $\sim 50\%$, if corrected for extinction and proper care is taken for UV flux contribution of AGNs (Kaviraj et al. 2006).

Early-type galaxies are known to have cold molecular gas (Huchtmeier, Sage & Henkel 1995; Morganti et al. 2006; Combes, Young & Bureau 2007; Oosterloo et al. 2010). More recently, in the ATLAS^{3D} sample of early-type galaxies the detection rate of molecular gas is $\sim 22\%$ with H_2 mass $\log M(H_2)/M_\odot$ in the range 7.10 - 9.29. A strong correlation between presence of molecular gas and dust, blue features and young stellar ages seen in the $H\beta$ absorption indicate that the detected molecular gas is often involved in the star formation (Young et al. 2011). Based on the CO emission in a representative sample of early-type galaxies, Combes, Young & Bureau (2007) and Crocker et al. (2011) showed that the CO-emitting early-type galaxies form a low star formation rate (SFR) extension to the empirical law in spirals.

We searched for available data on CO emission in our sample galaxies. Twelve out of 26 galaxies with dust and $H\alpha$ emission in our sample were mapped to check for CO emission while for remaining 14 galaxies we don't have any information. CO was detected in only four galaxies namely NGC 2768, NGC 3489 (Crocker et al. 2011) NGC 3607, NGC 5866 (Davis et al. 2011) and upper limits are available for NGC 4125 (Wiklind et al. 1995), NGC 4649 (Young 2002). Using $[OIII]/H\beta$ ratio Crocker et al. (2011) have investigated possible source of ionization in his sample galaxies. It is concluded that in NGC 2768 old pAGB stars/AGN and in NGC 3489 young pAGB stars are the main source of the ionizing photons. However, to get a better estimate of fraction of CO emitting galaxies, where star formation is the dominant source of ionization, a detailed investigation similar to that done by Crocker et al. (2011) is required.

4.3 Origin of dust and gas in early-type galaxies

In early-type galaxies presence of ISM in various forms is well established, but its origin is still an open issue. Many evidences support their co-existence and physical association, pointing towards a common origin (Goudfrooij et al. 1994b; Goudfrooij & de Jong 1995; Macchetto et al. 1996; Sarzi et al. 2006; Finkelman et al. 2010, 2012). As discussed earlier, $H\alpha$ emission is detected in a significant fraction of our sample galaxies. The matching morphology of line emitting regions with that of optical extinction indicates co-existence of dust and ionized gas in them. The possible sources for origin of dust and gas in these systems are internal and external. In case of internal origin dust is deposited through mass loss from evolved stars. The dust particles also get destroyed

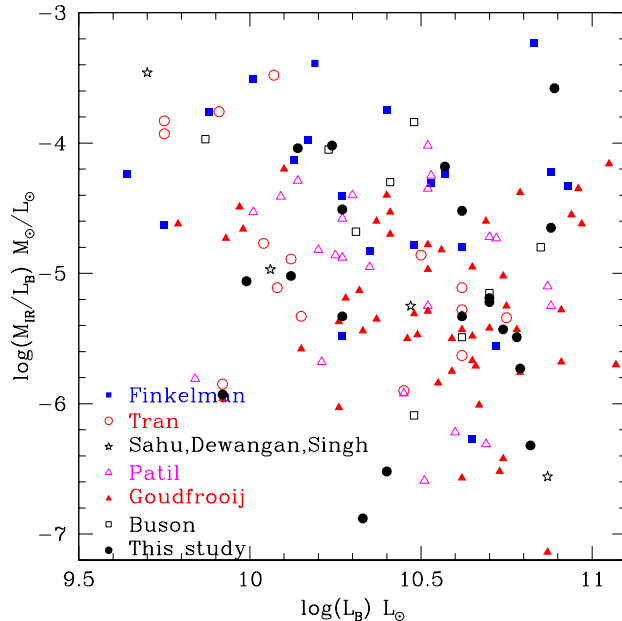


Fig. 6. Comparison IRAS dust mass, normalized by the luminosity

due to sputtering in various environments. It has been demonstrated that the mass of dust observed in early-type galaxies is generally higher than that expected from stellar mass loss, indicating an external origin of dust such as galaxy interaction or mergers (Goudfrooij & de Jong 1995; Patil et al. 2007; Finkelman et al. 2012 and references therein).

To investigate possible origin of dust in early-type galaxies relationship between optical luminosity and dust mass normalized by luminosity is also explored (Goudfrooij & de Jong 1995; Ferrari et al. 1999; Patil et al. 2007). In Figure 6, IRAS dust mass normalized with respect to blue luminosity is plotted against blue luminosity for the combined sample. The absence of any apparent correlation between these quantities suggests the possibility of external such as merger related origin of dust and gas in these galaxies.

The observed misalignment between the angular momentum vectors of interstellar gas and stellar system in several early-type galaxies suggests that they are kinematically decoupled (Bertola et al. 1988; Kim 1989; van Dokkum & Franx 1995; Caon, Macchetto & Pastoriza 2000; Krajnović et al. 2008; Sarzi et al. 2006). Further, Sarzi et al. (2006) showed that the kinematical misalignment between the gaseous and stellar component is strongly dependent on apparent flattening and the level of rotational support in these galaxies. The flatter and faster rotating early-type galaxies are known to have preferentially co-rotating gaseous and stellar systems, indicating that an internal origin of gas may play an important role in fast rotating galaxies. Hence, it is necessary to invoke a balance between the internal and external origin of gas and dust to explain the recent observational results (Finkelman et al. 2012). Moreover, the observed

blue colours (near-UV - $r < 5.5$) in a large sample of early-type galaxies can only be explained by introducing some amount of recent star formation in these galaxies (Kaviraj et al. 2006). The recycled gas from stellar mass loss within the galaxy is not enough to account for their observed blue colour. Hence, an additional source of fuel for star formation is unavoidable, may be from external origin.

5 Summary

We have explored the properties of dust and ionized gas in a sample of 40 nearby early-type galaxies using broad-band and narrow-band imaging data. The main findings of this work are summarized below

- (1) The value of R_V , the ratio between the total extinction in V band and the selective extinction $E(B - V)$ between B and V bands, for the sample galaxies derived using our observations lies in the range 2.1 - 3.8 with an average of 2.95.
- (2) The extinction curves derived for the sample galaxies run parallel to that of the canonical curve of our Galaxy, suggesting similar optical extinction properties of dust grains in extragalactic environment as that of the Milky Way. The relative size of the dust grains $\langle a \rangle / a_{Gal}$ in these galaxies is found to vary between 0.75 - 1.47.
- (3) Mass of dust calculated using the total optical extinction is in the range 10^2 to $10^4 M_\odot$, lower than those estimated using IRAS fluxes by a factor of $\sim 10^2$. This indicates that a significant fraction of dust is diffusely distributed, throughout the galaxy and remains undetected in optical observations.
- (4) The mass of the ionized gas lies in the range 7×10^2 - $5 \times 10^5 M_\odot$. The morphology of dust and ionized gas emission for these galaxies is found to be similar, implying their plausible physical association. Among various mechanism, at least in some of the early type galaxies star formation at a low level could be a major source of ionization, however more CO observations of $H\alpha$ emitting early-type galaxies are necessary to determine the source of the ionization in these galaxies.
- (5) The absence of any apparent correlation between the blue luminosity and normalized IRAS dust mass suggests the probability of merger related origin of dust and gas in these galaxies, over and above the internal origin through stellar mass loss.

Acknowledgments

We thank the anonymous referee for valuable comments which improved the scientific contents of the paper. SK, LKC and SKP are grateful to ISRO for financial support under RESPOND scheme (project no. ISRO/RES/2/343/2007-08). We thank the directors of IIA, Bangalore, IUCAA, Pune and the Time Allocation Committees for allotting the nights for our observations. SK is grateful to Prof. T.P. Prabhu and Prof. A.K. Kembhavi, for the local hospitality and use of computational facilities at CREST(IIA) and IUCAA, respectively. We acknowledge Dr. M. K. Patil and Dr. Sudhanshu Barway for their valuable suggestions. The authors are thankful to Late Prof. R.K. Thakur for his constant encouragement and moral support throughout this work. This research has made use of the NASA/IPAC Extragalactic Database (NED) which is operated by the Jet Propulsion Laboratory, California Institute of Technology, under contract with the National Aeronautics and Space Administration. This research has made use of NASA's Astrophysics Data System. We acknowledge the usage of the HyperLeda database (<http://leda.univ-lyon1.fr>).

References

- Bertola, F. & Galletta, G., 1978. *ApJ* 226, 115
Bertola, F., Galletta, G., Kotanyi, C., Zeilinger, W. W., 1988. *MNRAS* 234, 733
Brown, B. A. & Bregman, J. N., 1998. *ApJ* 495, L75
Buson, L. M., Sadler, E. M., Zeilinger, W. W., Bertin, G., Bertola, F., Danzinger, J., Dejonghe, H., Saglia, R. P., de Zeeuw, P. T., 1993. *A&A* 280, 409
Caon, N., Macchetto, D., Pastoriza, M., 2000. *ApJS* 127, 39
Canizares, C. R., Fabbiano, G., Trinchieri, G., 1987. *ApJ* 312, 503
Combes, F., Young, L. M., Bureau, M., 2007. *MNRAS* 377, 1795
Crocker, A. F. et al. (2011) *MNRAS*, 410, 1197
Davis, T. A., et al. (2011) *MNRAS*, 414, 968
de Koff, S. et al., 2000. *ApJS* 129, 33
de Vaucouleurs, G., de Vaucouleurs, A., Corwin, H. G., Buta, R. J., Paturel, G., Fouque, P., 1992. *Obs* 112, 127 Third Reference Catalogue of Bright Galaxies (New York:Springer)
Dewangan, G. C., Singh K. P., Bhat, P. N., 1999. *AJ* 118, 785
Draine, B. T. & Lee, H. M., 1984. *ApJ* 285, 89
Ebner K., Balick B., 1985. *AJ* 90, 183
Fabbiano, G., Gioia, I. M., Trinchieri, G., 1989. *ApJ* 347, 127
Ferrari, F., Pastoriza, M. G., Macchetto, F., Caon, N., 1999. *A&AS* 136, 269
Finkelman, I. et al., 2008. *MNRAS* 390, 969

- Finkelman, I., Brosch, N., Funes, J. G., Kniazev, A. Y., Väisänen, P., 2010. MNRAS 407, 2475
- Finkelman, I. et al., 2010. MNRAS 409, 727
- Finkelman, I., Brosch, N., Funes, J. G., Barway, S., Kniazev, A., Väisänen, P., 2012. MNRAS 422, 1384
- Forman, W., Jones, C., Tucker, W., 1985. ApJ 293, 102
- González-Serrano, J. I., Carballo, R., 2000. A&AS 142, 353
- Goudfrooij, P., Hansen, L., Jorgensen, H. E., Norgaard-Nielsen, H. U., 1994b. A&AS 105, 341
- Goudfrooij, P., de Jong T., Hansen L., Norgaard-Nielsen, H.U., 1994c. MNRAS 271, 833
- Goudfrooij, P., Hansen, L., Jorgensen, H. E., Norgaard-Nielsen, H. U., de Jong T., van den Hoek, L.B., 1994a. A&AS 104, 179
- Goudfrooij, P. & de Jong, T., 1995. A&A 298, 784
- Goudfrooij, P. & Trinchieri, G., 1998. A&A 330, 123
- Gunn, J. E., 1979. agn, book, 213
- Habe, A. & Ikeuchi, S., 1985. ApJ 289, 540
- Habe, A. & Ikeuchi, S., 1988. ApJ 326, 84
- Hawarden, T. G., Longmore, A. J., Tritton, S. B., Elson, R. A. W., Corwin, H. G., Jr., 1981. MNRAS 196, 747
- Hildebrand, R.H., 1983. QJRAS, 24, 267
- Hota, A., Rey, S., Kang, Y., Kim, S., Matsushita, S., Chung, J., 2012. MNRAS 422, L38
- Huchtmeier, W. K., Sage, L. J., Henkel, C., 1995. A&A 300, 675
- Jaffe, W., Ford, H. C., O'Connell, R. W., van den Bosch, F. C., Ferrarese, L., 1994. AJ 108, 1567
- de Jong T., Norgaard-Nielsen, H. U., Jorgensen, H. E., Hansen, L., 1990. A&A 232, 317
- Jura, M., 1982. ApJ 254, 70
- Kaviraj, S., Devriendt, J. E. G., Ferreras, I., Yi, S. K., Silk, J., 2006. arXiv:astro-ph/0602347
- Kaviraj, S. et al., 2012. MNRAS 423, 49
- Kennicutt, R. C., 1998. ARA&A 36, 189
- Kim, D., 1989. ApJ 346, 653
- Kim, D. & Fabbiano, G., 2003. ApJ 586, 826
- Kim, D. & Fabbiano, G., 2010. ApJ 721, 1523
- Krajnović, D. et al., 2008. MNRAS 390, 93
- Macchetto, F., Pastoriza, M., Caon, N., Sparks, W. B., Giavalisco, M., Bender, R., Capaccioli, M., 1996. A&AS 120, 463
- Mathis, J. S., Rumpl, W., Nordsieck, K. H., 1977. ApJ 217, 425
- Mathis, J. S., Wallenhorst, S. G., 1981. ApJ 244, 483
- Martel, A. R. et al., 2004. AJ 128, 2758
- Morganti, R. et al., 2006, MNRAS 371, 157
- Oke, J. B. & Schwarzschild, M., 1974, STIN, 7510879
- Oosterloo, T.A. et al., 2010. MNRAS 409, 500

- O'Sullivan, E., Forbes, D. A., Ponman, T. J., 2001. MNRAS 328, 461
- Patil, M. K., Pandey, S. K., Sahu, D. K., Kembhavi, A. K., 2007. A&A 461, 103
- Phillips, M. M., Jenkins, C. R., Dopita, M. A., Sadler, E. M., Binette, L., 1986. AJ 91, 1062
- Rieke, G. H. & Lebofsky, M. J., 1985. ApJ, 288, 618R
- Sadler, E. M. & Gerhard, O. E., 1985. MNRAS 214, 177
- Sahu, D. K., Pandey, S. K., Chakraborty, D. K., Kembhavi, A., Mohan, V. , 1996. A&A 314, 721
- Sahu, D. K., Pandey, S. K., Kembhavi, A., 1998. A&A 333, 803
- Sarzi, M. et al., 2006. MNRAS 366, 1151
- Sarzi, M. et al., 2010. MNRAS 402, 2187
- Sarazin, C. L., Irwin, J. A., Bregman, J. N., 2001. ApJ 556, 533
- Shields, J. C., 1991. AJ 102, 1314
- Singh, K. P., Bhat, P. N., Prabhu, T. P., Kembhavi, A. K., 1995. A&A 302, 658
- Spector, O., Finkelman, I., Brosch, N., 2012. MNRAS 419, 2156
- Spergel, D. N. et al. 2007. ApJS 170, 377
- Tem, P., Brighenti, F., Mathews, W. G., Bregman, J. D., 2004. ApJS 151, 237
- Thronson, H. A. & Telesco, C. M., 1986. ApJ 311, 98
- Tran, H. D., Tsvetanov, Z., Ford, H. C., Davis, J., Jaffe, W., van den Bosch, F. C., Rest, A., 2001. AJ 121, 2928
- Trinchieri, G. & di Serego Alighieri S., 1991. AJ 101, 1647
- van Dokkum, P. G. & Franx, M., 1995. AJ 110, 2027
- van Albada, T. S., Kotanyi, C. G., Schwarzschild, M., 1982. MNRAS 198, 303
- Veron-Cetty, M. P. & Veron, P., 1988. A&A 204, 28
- Waller, W. H., 1990. PASP, 102, 1217
- Wiklund, T., Combes, F., Henkel, C., 1995. A&A 297, 643
- Wise, M. W. & Silva, D. R., 1996. ApJ 461, 155
- Xilouris, E. M., Georgakakis, A. E., Misiriotis, A., Charmandaris, V., 2004. MNRAS 355, 57
- Young, J. S., Schloerb, F. P., Kenney, J. D., Lord, S. D., 1986b. ApJ 304, 443
- Young, L. M., 2002. AJ 124, 788
- Young, L. M. et al., 2011. MNRAS 414, 940